

Relativistic energy bands of (010) tungsten thin films

W. R. Grise, D. G. Dempsey,* Leonard Kleinman, and Kenneth Mednick

Department of Physics, The University of Texas, Austin, Texas 78712

(Received 7 June 1979)

We have made the first complete thin-film energy-band calculation including the spin-orbit interaction. Except for the inclusion of spin-orbit parameters, the method used is identical to the parametrization scheme we have previously applied to several $3d$ transition metals. Two of the three surface features observed in tungsten(001) photoemission are found near $\bar{\Gamma}$ as well as many other surface states throughout the two-dimensional Brillouin zone. Spin-orbit induced surface states are found in $\bar{\Gamma}$, \bar{X} , and \bar{M} gaps and an unexpected spin-orbit splitting of the degenerate surface states on opposite sides of the film is found and explained.

I. INTRODUCTION

The importance of the spin-orbit interaction in the surface electronic structure of tungsten has been a matter of contention¹ for several years. Of the two papers to address this question, one² calculated only the $\bar{\Gamma}_7$ irreducible representation and found a surface state in a spin-orbit induced gap. The other calculation³ was made throughout the two-dimensional Brillouin zone (2-D BZ), but included only d basis functions and hence failed to find all the interesting structure which is due to s - d hybridization. In particular it did not find any of the three surface resonance bands around $\bar{\Gamma}$ found in angle-resolved photoemission by Weng, Plummer, and Gustafsson⁴ at 0.3, 0.8, and 4.2 eV below E_F .

In this paper we compare the relativistic energy bands of a 39-layer W(010) film with and without the spin-orbit interaction. (We choose \hat{y} as the normal direction because with the spin quantization axis perpendicular to the film normal, the secular equation is real for \bar{K} along any symmetry line in the 2-D BZ as shown in the Appendix.) We use the same linear-combination-of-atomic-orbitals (LCAO) parametrization scheme that we previously applied to copper⁵ and nickel.⁶ Unlike the $3d$ transition metals, for tungsten we are able to find a set of parameters which not only fit the bulk energy bands but which also yield a charge neutral-surface without invoking any surface-parameter shifts. In Sec. II we describe how these parameters are obtained and in Sec. III we present the thin-film energy bands and planar densities of states, compare our results with the data of Weng *et al.*,⁴ and discuss an unexpected spin-orbit splitting of the degeneracy between surface states on opposite faces of the film.

II. PARAMETRIZATION

We have previously found that we could make excellent fits of calculated energy bands of $3d$

transition metals by parametrizing the Hamiltonian matrix elements between s , p , and d Wannier orbitals out to the third neighbor in the two-center approximation.⁷ However, when these parameters were used in thin-film calculations, surface charge deficits as large as 0.40 electrons/atom (δ) were found in Cu even though the d bands are filled and do not contribute to the deficit.⁵ This was caused by the fact that the appropriate surface orbitals have diagonal energies much lower than the bulk Wannier orbitals which have a large kinetic energy due to their orthogonality to Wannier orbitals on neighboring sites. Surface charge neutrality was obtained by lowering the bulk diagonal s and p parameters sufficiently. This corresponded to using orbitals that were about half way between Wannier and atomic orbitals but with the inclusion of overlap as well as Hamiltonian parameters we were able to obtain equally good fits for all choices of the s and p zeroth-neighbor parameters. A similar set of Ni parameters⁶ resulted in an sp surface deficit of 0.10 δ but a d surface surplus of 0.56 δ . Because we could not fit the bulk bands with an arbitrary choice of the zeroth-neighbor d parameter, we had to restore surface charge neutrality by making surface shifts of the zeroth-neighbor d parameter. The $3d$ parameters have two peculiarities: the degeneracy of the xy and $x^2 - y^2$ zeroth-neighbor parameters which should be split by the cubic crystal field is not, and the d - d and s - d overlap parameters are identically zero. These results are a consequence of Anderson's theorem⁸ which states that to first order in the overlap the potential from the neighboring atoms does not contribute to diagonal Hamiltonian matrix elements and the overlap does not enter the secular equation, i.e., there is a cancellation between the attractive potential and the kinetic energy of orthogonalization due to neighboring sites.

Our first step in fitting the relativistic energy bands of tungsten was to make a Wannier fit of the nonrelativistic energy bands of Petroff and Vis-

TABLE I. Relativistic set of spin-orbit, zeroth- and n th-neighbor Hamiltonian (H_n) parameters (Ry), and overlap (S_n) parameters for tungsten.

	$\zeta_p = 0.094\ 66$ H_1	$\zeta_d = 0.029\ 73$ H_2	$ss_0 = -0.099\ 96$ H_3	$pb_0 = 0.243\ 42$ S_1	S_2	$dd_0 = -0.273\ 55$ S_3
$ss\sigma$	-0.139 54	-0.057 51	-0.003 50	0.069 43	-0.000 54	0.000 29
$pp\sigma$	0.130 41	0.184 38	-0.000 00	-0.157 40	0.014 11	0.000 07
$pp\pi$	-0.002 58	0.000 53	-0.002 14	0.073 76	-0.009 97	-0.011 68
$dd\sigma$	-0.138 58	-0.068 26	0.015 52	0.117 50	-0.000 34	0.000 10
$dd\pi$	0.051 79	0.000 04	-0.006 49	-0.000 20	0.000 26	0.000 00
$dd\delta$	0.000 16	0.006 40	-0.000 00	0.000 01	-0.000 01	0.000 00
$sp\sigma$	0.174 19	0.099 25	-0.000 55	-0.103 45	-0.019 06	-0.000 40
$sd\sigma$	-0.119 24	-0.046 07	0.004 91	0.000 77	0.000 30	0.000 23
$pd\sigma$	-0.138 87	-0.121 84	0.010 60	0.109 99	0.000 32	0.000 00
$pd\pi$	0.045 91	0.001 78	0.003 38	-0.031 92	0.000 04	0.000 00

wanthan.⁹ Because the overlap of the $5d$ functions is not small, Anderson's theorem does not hold and the xy zeroth-neighbor parameter was 0.10 Ry greater than the $x^2 - y^2$. A thin-film calculation with these parameters led to a surface charge deficit of 0.466 δ and a surplus of 0.243 δ one layer in. We then refit the bulk energy bands with the inclusion of overlap. Although we were able to require that the xy and $x^2 - y^2$ zeroth-neighbor parameters take the same value, dd_0 , we could not obtain a good fit unless we let dd_0 be a free parameter. Because the splitting of the zeroth-neighbor degeneracy is caused by the potential from neighboring atoms, it was hoped that by letting the overlap cancel the splitting the effect of neighboring atoms on the zeroth-neighbor parameters could be removed¹⁰ and surface shifts would not be required. By adjusting ss_0 and pb_0 we were able to obtain both a good fit to the bulk energy bands and an essentially neutral-charge surfaces; we had a surface deficit of 0.031 δ and a 0.043 δ surplus one layer in.

Because the main relativistic effects are relative shifts of the different angular momentum components, and the spin-orbit interaction, we made a preliminary fit of the relativistic bands of Christensen and Feuerbacher¹¹ fixing all the parameters at their nonrelativistic values except for three semirigid band shift parameters¹² and two new spin-orbit parameters ζ_p and ζ_d , for the $\zeta \mathbf{L} \cdot \mathbf{S}$ term. Then using this set of parameters as starting values in our rms minimization routine we were able to rapidly fit the relativistic bands¹³ below¹⁴ 0.50 Ry at 50 points in the $\frac{1}{48}$ irreducible BZ with an rms error of 6.57×10^{-3} Ry. The final set of relativistic parameters is given in Table I. A major difference between these parameters and the nonrelativistic ones is that ss_0 is lower relative to dd_0 by 0.195 Ry in the relativistic case. Note that the largest third-neighbor parameters are an order of magnitude smaller than the largest

first-neighbor parameters and many of the third-neighbor parameters are completely negligible. Smallness of the third-neighbor parameters is a criterion for the adequacy of the parametrization.

III. PDOS AND ENERGY BANDS OF W(010)

Because the secular equation is complex, we were limited to a 27-layer film when calculating general points in the 2-D BZ. We performed the calculation at 91 points in the $\frac{1}{8}$ irreducible square 2-D BZ. We calculated the planar density of states (PDOS) using a Mulliken analysis as in Ref. 5 and 6 with a 0.003 Ry half-width Gaussian spread put on each energy level. Every energy was shifted by an additional -0.0165 Ry to obtain a Fermi energy (by integrating the total DOS up to 6 δ) of $E_F = -0.3353$ Ry in agreement with the work function¹⁵ $\Phi = 4.56$ eV. In Fig. 1 we show the PDOS for several planes and in Table II the planar charge density obtained by integrating the PDOS up to E_F together with the d component of that charge. The surface deficit and surplus one layer in are seen to be about five times larger than we obtained in the nonrelativistic film but taken together they give fairly good surface charge neutrality. A

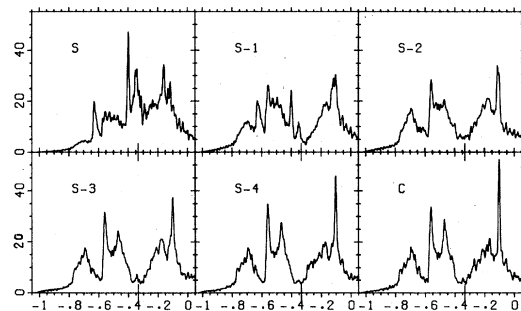


FIG. 1. Planar densities of states for central (C), surface (S), and next four interior planes (S- n) of relativistic tungsten including spin-orbit interaction.

TABLE II. Total and d component of charge on several planes in units of electrons per atom.

	ρ	ρ_d
S	5.8294	4.5348
S-1	6.2112	4.2541
S-2	5.9722	4.0605
S-3	6.0371	4.1211
S-4	5.9748	4.0528
C+1	5.9998	4.0768
C	5.9886	4.0648

small decaying oscillation is seen to exist from the second plane in all the way to the central plane. We believe a similar oscillation occurred in ρ in our 3d transition metal calculations but was an order of magnitude smaller and therefore

lost in the noise. We did notice in the 3d metals that the C and C + 2 PDOS tended to be identical but to have slight differences from the C + 1 and C + 3 PDOS. This long-range oscillation we believe is a consequence of not having screening in a non-self-consistent calculation. We also notice (by subtracting ρ_d from ρ) that we have 1.92 s and p electrons per atom in the center of the film and only 1.29 on the surface, i.e., there is a transfer of 0.46 δ from s and p to d in addition to the loss of 0.17 s and p electrons per atom in the surface plane. We believe some transfer of this sort does take place but we have no way of knowing how large it should be. We believe if we reduced it by refitting the bulk bands with lower values of ss_0 and pp_0 and by adding repulsive d surface parameters⁶ that the large charge oscillation on the first two surface planes would also be reduced.

In Fig. 2 we display the energy bands (shifted by -0.0165 Ry) of a 39-layer W(010) film calculated from the parameters of Table I with ξ_p and ξ_d set to zero. Although many of the features of these bands differ from the nonrelativistic bands we have calculated (but do not display), the two surface state bands observed in photoemission differ only slightly; hence the similarity in photoemission from Mo and W.

There is a surface state band of $\bar{\Sigma}_2$ and $\bar{\Delta}_1$ symmetry which extends arbitrarily close to $\bar{\Gamma}$ at -0.40 Ry = $E_F - 0.88$ eV but which does not exist at $\bar{\Gamma}$ even as a weak resonance. This band is found by Weng *et al.* at about $E_F - 0.8$ eV from about 2° off normal emission dispersing slightly upward with \bar{k} out to about halfway to the 2-D BZ zone boundary. Using polarized light they determined that for \bar{k} in the [11] direction, the wave function is odd under reflection in the plane of emission, i.e., has $\bar{\Sigma}_2$ symmetry. A recently reported¹⁶ self-consistent semirelativistic (i.e., no spin orbit) W calculation as well as a self-consistent Mo calculation,¹⁷ both report this surface state band disperses downward, contrary to our result and contrary to experiment. Because these calculations were performed on five- and seven-layer films, we repeated our calculation for films of this thickness and still obtained upward dispersing surface state bands. At -0.055 Ry ($E_F - 3.44$ eV) there is a $\bar{\Gamma}_1$ surface state which extends as a $\bar{\Sigma}_1$ surface state but as a $\bar{\Delta}_1$ resonance. This surface state is found at $E_F - 4.2$ eV by Weng *et al.* with $\bar{\Gamma}_1$ symmetry (it disappears with s polarized light). We do not have the $\bar{\Gamma}_1$ surface state by Weng *et al.*⁴ at about 0.4 eV below E_F . This state was found in the self-consistent W and Mo calculations.^{16,17} There are many additional surface states to be seen in Fig. 2 in gaps throughout the 2-D BZ. The $\bar{\Delta}_1$ - \bar{X}_3 - \bar{Y}_2 surface state band at about -0.64 Ry is only slight-

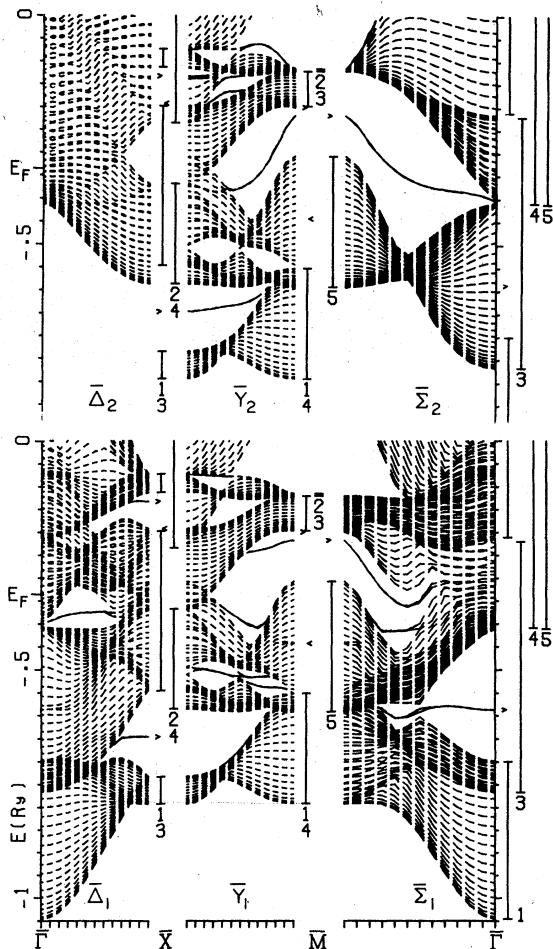


FIG. 2. Energy bands of 39-layer relativistic W(010) film with spin-orbit parameters set to zero. Where two symmetries span the same energy range, the left-pointing arrowhead indicates a surface state of the lower index symmetry. Surface state bands are represented by solid lines.

ly dispersive, is in a wide gap, has 90% of its charge density on the surface and first interior planes, and, as can be seen in Fig. 3, is not strongly affected by the spin-orbit interaction. It should contribute one of the strongest peaks in angle resolved photoemission but thus far has not been observed. This surface state band appears only as a short dispersive $\bar{\Delta}_1$ - \bar{X}_3 surface state band in a narrow gap in our nonrelativistic W calculation and appears not at all in the Mo calculation¹⁷; thus relativistic effects other than spin orbit can be important.

If we compare surface state bands in Figs. 2 and 3, we see, except for the one just discussed which has mainly *s* character, that they are all spin-orbit split. At first sight this is very surprising. Without spin orbit, surface states which are even and odd under \hat{y} reflection (remember \hat{y} is the film normal direction) are degenerate in a film this thick and can be added and subtracted to obtain the surface state localized on one surface or the other. With the inclusion of spin there is a fourfold degeneracy. It would appear that spin-orbit coupling could not lift this degeneracy because the fact that two-dimensional Bloch functions generally have no angular momentum implies the degeneracy of the two spin states on one surface and the fact that the two surfaces are identical and far enough apart that surface states on opposite surfaces have negligible overlap implies that surface states on opposite faces are degenerate in pairs. The fallacy in this logic is due to our not including spin *ab initio*. Consider, for example, the general point basis functions $x_n + ix_{\bar{n}}$ and $i(y_n - iy_{\bar{n}})$ (see Appendix) for $n=m$ and \bar{m} . The two x_m (y_m) functions go into $-i$ ($+i$) times themselves under the \hat{y} reflection, i.e., they are not even and odd, and hence cannot be combined to give basis functions containing only m or \bar{m} . Thus the surface states containing these basis functions cannot be combined to give states localized on a single surface and the fact that the surface state containing $x_m + ix_{\bar{m}}$ overlaps the surface state containing $i(y_{\bar{m}} - iy_m)$ allows the spin-orbit interaction to split this degeneracy. There still remains the Kramers degeneracy, however, and one can combine these surface states with their Kramers degenerate partner to obtain the surface states located on one surface or the other. For example,

$$-iIT(x_m + ix_{\bar{m}}) = x_m - ix_{\bar{m}},$$

where *I* and *T* are inversion and time reversal. Similar though more complicated arguments¹⁸ may be made for \bar{k} along $\bar{\Delta}$, \bar{Y} , or $\bar{\Sigma}$. At the symmetry points $\bar{\Gamma}$, \bar{X} , and \bar{M} , inversion is a member of the group of the wave vector. Because, unlike the \hat{y} reflection, inversion does not flip the spin, the

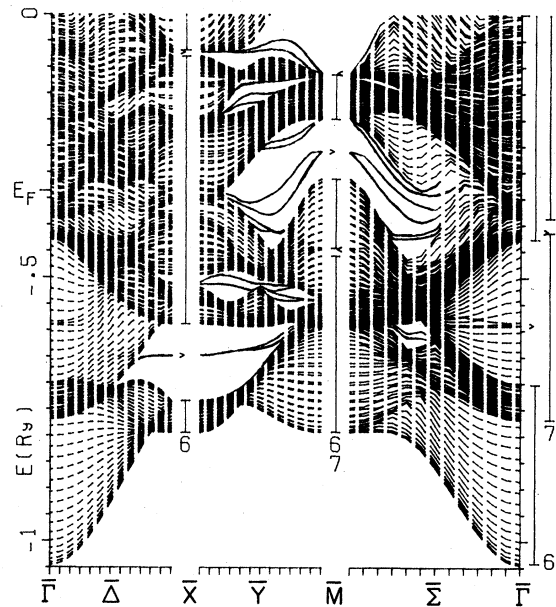


FIG. 3. Energy bands of a 39-layer relativistic W(010) film including spin-orbit coupling. At \bar{M} the left-pointing arrowheads indicate \bar{M}_6 surface states and the right pointing indicates an \bar{M}_7 surface state. Surface state bands are represented by solid lines.

basis functions and eigenfunctions at these points are either even or odd under inversion. The even and odd eigenfunctions, if they are surface state eigenfunctions, must be degenerate and may be combined to form surface states on one surface or the other. The Kramers degeneracy still remains to yield altogether a fourfold degeneracy. We see in Fig. 3 that the splitting of the surface state bands disappears at the symmetry points.

A single spin-orbit induced gap exists at each of the symmetry points in Fig. 3. Each of these gaps contains a single fourfold degenerate set of surface states. It appears to be a general rule that spin-orbit gaps contain a single set of surface states¹⁹ and that as one varies the surface parameters to force the surface states out of the top of the gap another set of surface states is forced out of the lower continuum into the bottom of the gap.²

Finally, we look at the effect of spin-orbit coupling on the experimentally observed surface features. The $\bar{\Delta}_1$ - $\bar{\Sigma}_2$ surface state band which pinches off at $\bar{\Gamma}$ becomes a fairly strong resonance band with much less dispersion. The upward dispersion along $\bar{\Delta}$ is less than 0.20 eV and along $\bar{\Sigma}$ less than 0.08 eV in good agreement with Weng *et al.*⁴ Our $\bar{\Gamma}_1$ surface state now becomes a very sharp resonance in both the $\bar{\Delta}$ and $\bar{\Sigma}$ directions. Along $\bar{\Delta}$ it broadens (in energy) and disappears about 30% of the way to \bar{X} ; along $\bar{\Sigma}$ it remains very sharp but spin orbit splits with nonresonant states between

the split pair which extend almost half way to \bar{M} . At $\bar{k}=0.26 \text{ \AA}^{-1}$ along the $\bar{\Sigma}$ direction, Weng *et al.*⁴ find the resonance at $E_F - 0.8 \text{ eV}$ to be very strong when the vector potential \bar{A} is perpendicular to \bar{k} but to still exist as a weak shoulder when \bar{A} is parallel to \bar{k} . Without spin orbit the resonance would completely disappear in the latter configuration, but we find that due to spin orbit, the basis functions that are even under reflection in the plane of emission are mixed in with about half the density (in a Mulliken analysis) of the odd basis

functions on the surface plus first interior planes of the surface resonant eigenfunctions.

In conclusion, we have calculated the relativistic energy bands of a 39-layer W(010) film obtaining surface charge neutrality without making any surface adjustments to the LCAO parameters which were obtained by fitting the bulk energy bands. We obtained two of the three experimentally observed surface features and explained several important spin-orbit effects on the surface electronic structure.

TABLE III. Basis functions at all points in the 2-D BZ. At \bar{X} and \bar{Y} the upper and lower signs apply to basis functions on the A and B planes respectively. At \bar{M} subscripts are used to indicate the type of plane and elsewhere the same basis functions appear on both A and B planes. At $\bar{\Delta}$ and the general point, $N \geq n \geq \bar{N}$, whereas elsewhere, $N \geq n \geq 0$ for a $2N+1$ layer film. T is the time reversal operator. Spin is quantized along \hat{z} and \hat{y} is the surface normal direction.

$$\begin{aligned} \text{General point: } & i(s_{n\uparrow} + i s_{\bar{n}\downarrow}), (x_{n\uparrow} + i x_{\bar{n}\downarrow}), i(y_{n\uparrow} - i y_{\bar{n}\downarrow}), (z_{n\uparrow} + i z_{\bar{n}\downarrow}), \\ & (x y_{n\uparrow} - i x y_{\bar{n}\downarrow}), i(x z_{n\uparrow} + i x z_{\bar{n}\downarrow}), (y z_{n\uparrow} - i y z_{\bar{n}\downarrow}), i[(x^2 - y^2)_{n\uparrow} + i(x^2 - y^2)_{\bar{n}\downarrow}], \\ & i[(3z^2 - r^2)_{n\uparrow} + i(3z^2 - r^2)_{\bar{n}\downarrow}]. \\ \bar{\Delta}_6: & i s_{n\uparrow}, x_{n\uparrow}, i y_{n\uparrow}, z_{n\uparrow}, x y_{n\uparrow}, i x z_{n\uparrow}, y z_{n\uparrow}, i(x^2 - y^2)_{n\uparrow}, i(3z^2 - r^2)_{n\uparrow}. \\ \bar{X}_6^+: & i(s_{n\uparrow} \pm s_{\bar{n}\downarrow}), (x_{n\uparrow} \mp x_{\bar{n}\downarrow}), i(y_{n\uparrow} \mp y_{\bar{n}\downarrow}), (z_{n\uparrow} \mp z_{\bar{n}\downarrow}), (x y_{n\uparrow} \pm x y_{\bar{n}\downarrow}), \\ & i(x z_{n\uparrow} \pm x z_{\bar{n}\downarrow}), (y z_{n\uparrow} \pm y z_{\bar{n}\downarrow}), i[(x^2 - y^2)_{n\uparrow} \pm (x^2 - y^2)_{\bar{n}\downarrow}], i[(3z^2 - r^2)_{n\uparrow} \pm (3z^2 - r^2)_{\bar{n}\downarrow}]. \\ \bar{X}_6^-: & i(s_{n\downarrow} \mp s_{\bar{n}\uparrow}), (x_{n\downarrow} \pm x_{\bar{n}\uparrow}), i(y_{n\downarrow} \pm y_{\bar{n}\uparrow}), (z_{n\downarrow} \pm z_{\bar{n}\uparrow}), (x y_{n\downarrow} \mp x y_{\bar{n}\uparrow}), \\ & i(x z_{n\downarrow} \mp x z_{\bar{n}\uparrow}), (y z_{n\downarrow} \mp y z_{\bar{n}\uparrow}), i[(x^2 - y^2)_{n\downarrow} \mp (x^2 - y^2)_{\bar{n}\uparrow}], i[(3z^2 - r^2)_{n\downarrow} \mp (3z^2 - r^2)_{\bar{n}\uparrow}]. \\ \bar{Y}_6: & \bar{X}_6^+ + \bar{X}_6^- \\ \bar{M}_{6A}^+, T\bar{M}_{7A}^+, \bar{\Gamma}_6^+: & i(s_{n\uparrow} + s_{\bar{n}\uparrow}), i(y_{n\uparrow} - y_{\bar{n}\uparrow}), [(x_{n\uparrow} - x_{\bar{n}\uparrow}) - (z_{n\uparrow} - z_{\bar{n}\uparrow})], \\ & [(x y_{n\uparrow} + x y_{\bar{n}\uparrow}) - (y z_{n\uparrow} + y z_{\bar{n}\uparrow})], i\{\sqrt{3} [(x^2 - y^2)_{n\uparrow} + (x^2 - y^2)_{\bar{n}\uparrow}] + [(3z^2 - r^2)_{n\uparrow} + (3z^2 - r^2)_{\bar{n}\uparrow}]\}. \\ \bar{M}_{6B}^-, T\bar{M}_{7B}^-, \bar{\Gamma}_6^-: & i(s_{n\downarrow} - s_{\bar{n}\downarrow}), i(y_{n\downarrow} + y_{\bar{n}\downarrow}), [(x_{n\downarrow} + x_{\bar{n}\downarrow}) + (z_{n\downarrow} + z_{\bar{n}\downarrow})], \\ & [(x y_{n\downarrow} - x y_{\bar{n}\downarrow}) + (y z_{n\downarrow} - y z_{\bar{n}\downarrow})], i\{\sqrt{3} [(x^2 - y^2)_{n\downarrow} - (x^2 - y^2)_{\bar{n}\downarrow}] + [(3z^2 - r^2)_{n\downarrow} - (3z^2 - r^2)_{\bar{n}\downarrow}]\}. \\ T\bar{M}_{6B}^+, \bar{M}_{7B}^+, \bar{\Gamma}_7^+: & [(x_{n\uparrow} - x_{\bar{n}\uparrow}) + (z_{n\uparrow} - z_{\bar{n}\uparrow})], [(x y_{n\uparrow} + x y_{\bar{n}\uparrow}) + (y z_{n\uparrow} + y z_{\bar{n}\uparrow})], \\ & i(x z_{n\uparrow} + x z_{\bar{n}\uparrow}), i\{[(x^2 - y^2)_{n\uparrow} + (x^2 - y^2)_{\bar{n}\uparrow}] - \sqrt{3} [(3z^2 - r^2)_{n\uparrow} + (3z^2 - r^2)_{\bar{n}\uparrow}]\}. \\ T\bar{M}_{6A}^-, \bar{M}_{7A}^-, \bar{\Gamma}_7^-: & [(x_{n\downarrow} + x_{\bar{n}\downarrow}) - (z_{n\downarrow} + z_{\bar{n}\downarrow})], [(x y_{n\downarrow} - x y_{\bar{n}\downarrow}) - (y z_{n\downarrow} - y z_{\bar{n}\downarrow})], \\ & i(x z_{n\downarrow} - x z_{\bar{n}\downarrow}), i\{[(x^2 - y^2)_{n\downarrow} - (x^2 - y^2)_{\bar{n}\downarrow}] - \sqrt{3} [(3z^2 - r^2)_{n\downarrow} - (3z^2 - r^2)_{\bar{n}\downarrow}]\}. \\ \bar{\Sigma}_6: & i(s_{n\uparrow} + s_{\bar{n}\uparrow}), i[(s_{n\uparrow} - s_{\bar{n}\uparrow}) - (s_{n\downarrow} - s_{\bar{n}\downarrow})], [(x_{n\uparrow} + x_{\bar{n}\uparrow}) + (z_{n\uparrow} + z_{\bar{n}\uparrow})], \\ & [(x_{n\uparrow} - x_{\bar{n}\uparrow}) + (z_{n\uparrow} + z_{\bar{n}\uparrow}) - (x_{n\downarrow} - x_{\bar{n}\downarrow}) - (z_{n\downarrow} - z_{\bar{n}\downarrow})], [(x_{n\uparrow} + x_{\bar{n}\uparrow}) \\ & - (z_{n\uparrow} + z_{\bar{n}\uparrow})], [(x_{n\uparrow} - x_{\bar{n}\uparrow}) - (z_{n\uparrow} - z_{\bar{n}\uparrow}) + (x_{n\downarrow} - x_{\bar{n}\downarrow}) - (z_{n\downarrow} - z_{\bar{n}\downarrow})], \\ & i(y_{n\uparrow} - y_{\bar{n}\uparrow}), i[(y_{n\uparrow} + y_{\bar{n}\uparrow}) - (y_{n\downarrow} + y_{\bar{n}\downarrow})], [(x y_{n\uparrow} - x y_{\bar{n}\uparrow}) + (y z_{n\uparrow} - y z_{\bar{n}\uparrow})], \\ & [(x y_{n\uparrow} + x y_{\bar{n}\uparrow}) + (y z_{n\uparrow} + y z_{\bar{n}\uparrow}) - (x y_{n\downarrow} + x y_{\bar{n}\downarrow}) - (y z_{n\downarrow} + y z_{\bar{n}\downarrow})], [(x y_{n\uparrow} - x y_{\bar{n}\uparrow}) \\ & - (y z_{n\uparrow} - y z_{\bar{n}\uparrow})], [(x y_{n\uparrow} + x y_{\bar{n}\uparrow}) - (y z_{n\uparrow} + y z_{\bar{n}\uparrow}) + (x y_{n\downarrow} + x y_{\bar{n}\downarrow}) - (y z_{n\downarrow} + y z_{\bar{n}\downarrow})], \\ & i(x z_{n\uparrow} + x z_{\bar{n}\uparrow}), i[(x z_{n\uparrow} - x z_{\bar{n}\uparrow}) - (x z_{n\downarrow} - x z_{\bar{n}\downarrow})], i\{[(x^2 - y^2)_{n\uparrow} + (x^2 - y^2)_{\bar{n}\uparrow}] \\ & - \sqrt{3} [(3z^2 - r^2)_{n\uparrow} + (3z^2 - r^2)_{\bar{n}\uparrow}]\}, i\{[(x^2 - y^2)_{n\uparrow} - (x^2 - y^2)_{\bar{n}\uparrow}] - \sqrt{3} [(3z^2 - r^2)_{n\uparrow} \\ & - (3z^2 - r^2)_{\bar{n}\uparrow}] + [(x^2 - y^2)_{n\downarrow} - (x^2 - y^2)_{\bar{n}\downarrow}] - \sqrt{3} [(3z^2 - r^2)_{n\downarrow} - (3z^2 - r^2)_{\bar{n}\downarrow}]\}, \\ & i\{\sqrt{3} [(x^2 - y^2)_{n\uparrow} + (x^2 - y^2)_{\bar{n}\uparrow}] + [(3z^2 - r^2)_{n\uparrow} + (3z^2 - r^2)_{\bar{n}\uparrow}]\}, i\{\sqrt{3} [(x^2 - y^2)_{n\uparrow} - (x^2 - y^2)_{\bar{n}\uparrow}] \\ & + [(3z^2 - r^2)_{n\uparrow} - (3z^2 - r^2)_{\bar{n}\uparrow}] - \sqrt{3} [(x^2 - y^2)_{n\downarrow} - (x^2 - y^2)_{\bar{n}\downarrow}] - [(3z^2 - r^2)_{n\downarrow} - (3z^2 - r^2)_{\bar{n}\downarrow}]\} \end{aligned}$$

ACKNOWLEDGMENT

This research was supported by the NSF under Grant No. DMR 77-21559.

APPENDIX

Because real-space matrix elements between 2-D Bloch basis functions contain a factor $\cos k \cdot \bar{R}_i$ or $i \sin k \cdot \bar{R}_i$ depending upon whether the basis functions have like or unlike symmetry under the twofold rotation about the normal axis, one can make these matrix elements real by including a factor of i in either the even or the odd basis functions. On the other hand, spin-orbit matrix elements between p orbitals and between d orbitals are real when y , xz , $x^2 - y^2$, and $3z^2 - r^2$ contain a factor of i . Thus it appears that if y is chosen as the surface normal direction with spin quantized in the \hat{z} direction, the factors of i may be included to make the real-space and spin-orbit matrix elements simultaneously real. This turns out to be the case whenever there is at least one nontrivial symmetry operation in the group of the 2-D wave vector, but is not true at a general point

of the 2-D BZ. Even at the general point, however, the secular equation is somewhat simpler for \hat{y} normal.

In Table III we list the basis functions obtained by using the projection operator and the double group character tables given by Lax.²⁰ At the general point where one has only the identity and \hat{y} reflection, there are two one-dimensional irreducible representations, degenerate by time reversal. The form of the basis functions, e.g., $x_n = x_{n_1} + ix_{n_2}$, insures that the real-space matrix elements are real and that the matrix elements between, say, x_n and y_{n-1} or y_{n-2} are independent of n whereas without spin that is not the case because of the overlap of orbitals on the n and \bar{n} planes when n is small. Thus the real-space part of the secular matrix is constructed out of repeated zero-, first-, and second-neighbor plane Bloch function submatrices. Because of the i multiplying the \dagger orbitals, spin-orbit matrix elements between x_n and $z_{\bar{n}} = z_{n_1} + iz_{n_2}$ are pure imaginary. Along all symmetry lines and at high symmetry points the irreducible representations are all two dimensional, there are no internal factors of i in the basis functions, and the secular matrices are completely real.

*Present address: Bell Labs, Naperville, Ill. 60540.

¹R. W. Kasowski, *Solid State Commun.* **17**, 179 (1975).

²R. Feder and K. Sturm, *Phys. Rev. B* **12**, 537 (1975).

³O. Bisi, C. Calandra, P. Flaviani, and F. Manghi, *Solid State Commun.* **21**, 121 (1977).

⁴S. L. Weng, E. W. Plummer, and T. Gustafsson, *Phys. Rev. B* **18**, 1718 (1978).

⁵K. S. Sohn, D. G. Dempsey, and L. Kleinman, *Phys. Rev. B* **16**, 5367 (1977).

⁶(a) D. G. Dempsey, W. R. Grise, and L. Kleinman, *Phys. Rev. B* **18**, 1270 (1978); (b) **18**, 1550 (1978).

⁷J. C. Slater and G. F. Koster, *Phys. Rev.* **94**, 1498 (1954).

⁸P. W. Anderson, *Phys. Rev.* **181**, 25 (1969).

⁹I. Petroff and C. R. Viswanthan, *Phys. Rev. B* **4**, 799 (1971).

¹⁰Perhaps the best that can be hoped for is that this technique removes the contribution of the neighboring sites to the $l=4$ Kubic harmonic of the potential from which the zeroth-neighbor parameter would be calculated in a first principles calculation.

¹¹N. E. Christensen and B. Feuerbacher, *Phys. Rev. B* **10**, 2349 (1974).

¹²See Eq. (1) of Ref. 6(a).

¹³We first shifted all the energies in Table II of Ref. 10 by -1.2050 Ry to obtain a Fermi energy close to the negative of the work function.

¹⁴If a level lay below 0.50 Ry in either the shifted bands of Ref. 10 or in our fit to them it was included in the rms error.

¹⁵G. A. Somorjai, *Solid State Chemistry and Physics*, edited by P. F. Weller (Dekker, New York, 1974), Vol. 2, pp. 667-720.

¹⁶M. Posternak, H. Krakauer, A. J. Freeman, and D. D. Koeling, *Bull. Am. Phys. Soc.* **24**, 439 (1979).

¹⁷G. P. Kerker, K. M. Ho, and M. L. Cohen, *Phys. Rev. Lett.* **40**, 1593 (1978).

¹⁸For example to show that at \bar{Y} a surface state can be localized on a single surface by combining a surface state eigenfunction with its Kramers degenerate partner one must use the following facts. The basis functions at \bar{Y} are either even (\bar{X}_6^+ type) or odd (\bar{X}_6^- type) under inversion. In general, the coefficient of the even and odd basis functions in an eigenfunction are completely arbitrary but if the eigenfunction is a surface state, the coefficients of the even and odd basis functions are equal in pairs.

¹⁹J. B. Pendry and S. J. Gurman, *Surf. Sci.* **49**, 87 (1975). [Note that one of us has claimed that some of the other conclusions drawn in this paper are not correct. See L. Kleinman, *Phys. Rev. B* **13**, 4640 (1976).]

²⁰M. Lax, *Symmetry Principles in Solid State and Molecular Physics* (Wiley, New York, 1974).